Multifunction Wide-Band Array Design

Chris Hemmi, *Senior Member, IEEE*, R. Thomas Dover, Fred German, and Anthony Vespa

(Invited Paper)

***Abstract*— High-performance active arrays operating over C, X, and Ku-band have been demonstrated using newly developed designs of wide-band radiating elements and wide-band monolithic microwave integrated circuits (MMIC's). The advanced shared aperture program (ASAP) explored the development of wide-band multifunction arrays capable of simultaneous and time interleaved radar, electronic warfare, and communications functions. Two iterations of radiating element and transmit/receive (T/R) module design were completed during this program. Radiating aperture design approach, overall array concepts, and current design technology and performance are summarized in this paper.**

***Index Terms*— Antenna arrays.**

I. ASAP System Concept

THE Navy funded a series of studies and development programs from 1985 to develop broad-band phased-array technology for application to strike/fighter aircraft. From 1990 to 1994, the Navy funded the Defense Systems and Electronics Group of Texas Instruments Inc. (now a part of the Raytheon Systems Company) for the development of designs for the array and T/R module. Small test arrays and prototype modules were built and evaluated. These studies concentrated on apertures with continuous coverage of C band through Ku band. A strike/fighter aircraft with broad-band array apertures which are shared between radar, passive electronic support measures (ESM), active electronic counter measures (ECM), and communications functions has:

- greater flexibility for multiple missions and multiple roles;
- increased effectiveness and enhanced countermeasure capabilities;
- improved survivability;
- reduced weight and cost.

The advanced shared aperture program (ASAP) is designed as a broad-band multifunction array which provides continuous operation over upper C, X, and Ku bands. The array is intended for shared sequential or simultaneous operation for airborne radar, ESM, ECM, and communications. For a tactical aircraft, forward-looking nose-mounted arrays with several thousand radiating elements and smaller side/rear looking arrays with several hundred elements are envisioned for full azimuth coverage. Fig. 1 is a layout of a candidate nose-aperture design with shading distinguishing the active section (populated with T/R modules) and the sections populated with passive, terminated radiating elements. For a tactical aircraft, the size and approximate elliptical shape of the active part of the forward aperture is set by radar sidelobe, resolution, gain, and transmit power requirements. The outer shape is configured for meeting radar cross section (RCS) requirements by adding terminated radiating elements around the active elements.

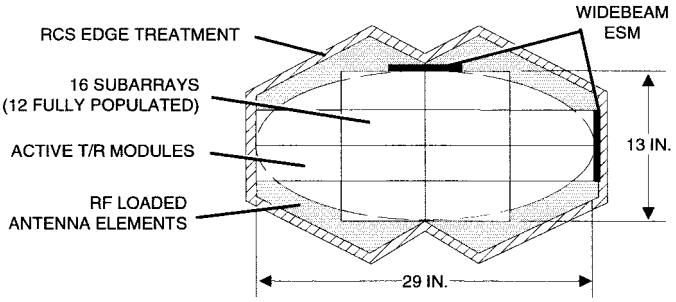

Fig. 1. Forward aperture layout.

The ASAP concept makes the substantial antenna gain and transmitter capability required for the forward looking radar functions, available for other microwave frequency electronic warfare and communications functions. The nose array is partitioned into subarrays (as illustrated in Fig. 1) to allow aperture size to be tailored to the function's needs and to support operation of several functions simultaneously. Linear array sections along the top and side are dedicated to wide-beam antenna functions One standard wide-beam function for tactical aircraft is a wide field-of-view phase interferometer [1]. These linear array sections also include a few array elements devoted to sidelobe canceler or guard-horn functions [2]. By using small sections of array elements for these functions, the RCS performance of the aperture is maintained.

A set of broad-band apertures such as this can perform the many RF functions required on modern tactical aircraft over the upper part of the microwave frequency band. The ASAP concept could be extended to ultra high frequency (UHF) and lower frequency bands by developing a similar broad-band module and array design for lower microwave frequency bands. Specifics of this are not covered further in this paper. This use of shared apertures will result in significant savings in weight and prime power. Overall acquisition and life-cycle costs are expected to be lower than current approaches with multiple single-function apertures. Shared operation will make practical added functions such as self-protect ECM or directive microwave data links which are desirable but have heretofore rarely been practical or affordable on tactical aircraft.

Manuscript received June 11, 1997; revised June 10, 1998. This work was supported in part by NAVAIR, Washington, DC, under Contracts N62269-92-C-0508 and N00019-91-C-0210. Program and project managers were C. Capasell and M. Fenton, respectively.

The authors are with Raytheon Systems Company, McKinney, TX 75070 USA.

Publisher Item Identifier S 0018-926X(99)04422-1.

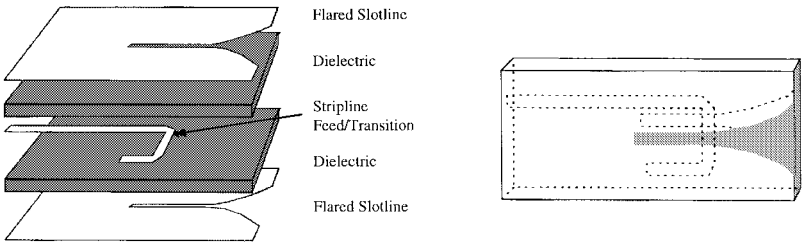

Fig. 2. Single flared-notch antenna element. (a) Exploded view showing layered construction. (b) Side view of assembled element.

II. Radiating Aperture Design

The radiating aperture for ASAP requires wide bandwidth (C band through Ku band), multiple polarization, wide-angle beam scan, and low RCS. The aperture design uses a square-element grid with horizontal and vertical flared-notch radiators at each element position. The wide-angle beam scan at the highest frequency requires an element spacing of less than 0.4 in. Control of Bragg scattering lobe location drives the spacing even smaller than required for beam scan; to half a wavelength at the Ku band highest frequency. A flared-notch antenna element was chosen for ASAP. This type of element is commonly used in wide-band arrays [3] due to its relatively small size (allowing it to fit into the aperture grid) and wide-band performance. Printed circuit fabrication techniques make the element easy to construct and configuring orthogonal elements to realize the dual polarization requirement is relatively straightforward. The element consists of three conductive layers with the inner layer forming the stripline feed and transition and the outer metal layers realizing the flared slotline for the radiating portion. Fig. 2 shows the layered construction of a single flared-notch element.

A. Design Process

"Traditional" design methodologies for phased-array antenna elements often leaves the antenna designer taking a best guess at an element and feed design using information obtained from simplified lumped element models and past experience. This usually leads to several candidate element designs that are built and tested in waveguide simulators to find the "best" element. This approach places a severe limit on the number of design iterations that can be tried due to time constraints and the cost of building many different elements for testing.

In the past decade rapid advances in computer hardware coupled with the availability of reliable computational electromagnetic field solvers has led to drastic reduction in design cycle times. Hardware design iterations that were once limited by time and cost can now often be performed on the computer quickly and at minimal cost. In the time it would take to build and test just a few candidate elements in waveguide simulators literally hundreds of different element design could be simulated on the computer.

The numerical method used for the simulations in this work was the transmission line matrix (TLM) method [4]. The TLM method is a three-dimensional (3-D) volumetric time domain method that provides a full temporal field solution to the Maxwell equations. The time-domain nature of the technique makes it ideally suited to the characterization of broad-band devices since results over the entire frequency band can be obtained in a single simulation. Arbitrary geometries and material inhomogeneities are easily accounted for in the method allowing the complete element and feed as well as the array support structure to be modeled accurately.

The approach used was to model the entire element and feed in various waveguide simulators using our TLM simulator. These models include the effects of element to element mutual coupling in an infinite planar array environment. since these models mimic the actual hardware waveguide simulators they are subject to the same restrictions in terms of the frequency and scan angle ranges that can be characterized [5]. Unlike hardware waveguide simulators however, implementing waveguides with various combinations of perfect electric conductors and perfect magnetic conductors for the waveguide walls is possible in the computer models. This leads to many more frequency/scan angle combinations that can be modeled on the computer as compared to hardware measurements.

B. Element Design

In order to arrive at an acceptable design an element used in a previous phase of the ASAP program was used as a baseline. This particular design was arrived at without the benefit of electromagnetic simulation to characterize performance and was lacking in several respects. It consisted of a second-order stripline-to-slotline transition and a circular taper for the flared-notch radiator. In order to improve performance TLM models of various improvements to this baseline element were constructed and characterized in different sized waveguide simulators. Fig. 3 illustrates the basic computational model for a two element waveguide simulator. It consists of two flared-notch elements (the stripline feed and transition is also included in the model though not visible in the figure) in a rectangular waveguide. The model includes the metal posts that are present in the actual array structure to hold the elements in place. A relatively coarse mesh was used to discretize the problem (for example only three TLM cells were used across the width of the stripline conductor) in order to minimize simulation time.

The waveguide end of the simulator is excited with the fundamental mode while the stripline feeds are terminated with a matched load. The resulting reflection coefficient is calculated over the entire band of the waveguide via a Fourier transform of the time-domain reflected field. The design criteria was to minimize this reflection coefficient over the band of interest. In

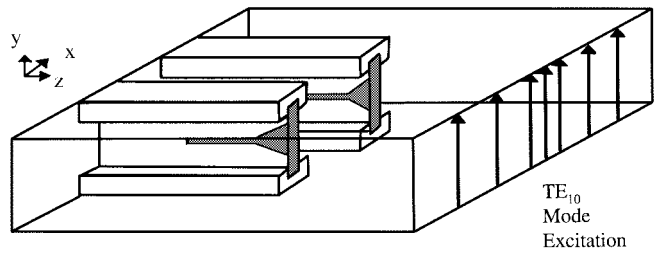

Fig. 3. Model of two-element waveguide simulator.

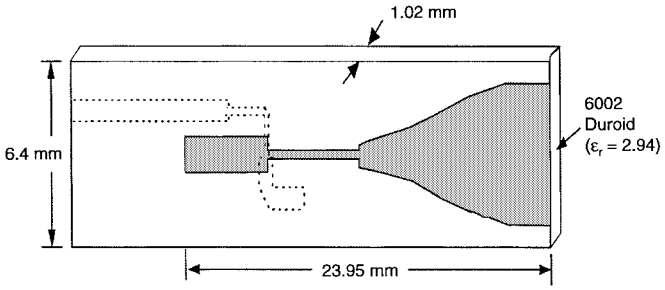

Fig. 4. Final element design with Klopfenstein–Hecken flared slotline radiator and fourth-order Marchand balun for stripline-to-slotline transition.

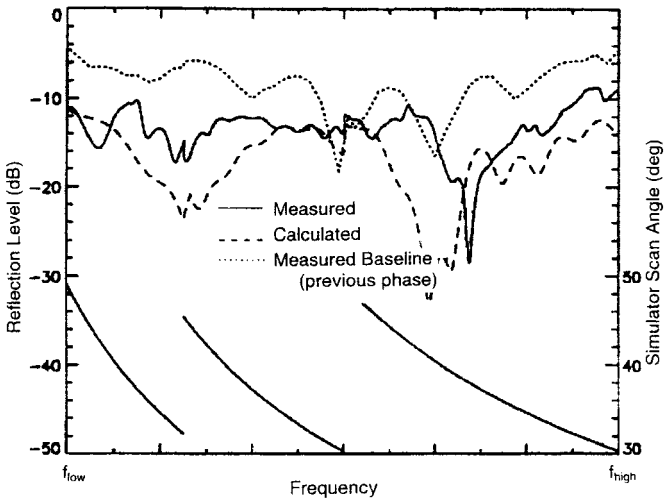

Fig. 5. Waveguide simulator return loss for final element design. Lower curves show frequency dependence of H-plane scan angle in three different simulators.

order to cover the entire $3:1$ bandwidth, waveguide simulators with two, three, and four radiating elements were simulated.

Since the actual array is dual polarized, there are also horizontal elements present which are not included in the waveguide simulator. There are difficulties associated with including these in the waveguide simulator because the waveguide walls that form the symmetry boundaries on the top and bottom short out the stripline feeds on the horizontally polarized elements. (Note that this is a limitation of waveguide simulators in general and not the computational model). Extensive studies were performed to include the horizontal elements. For example, the radiating portion of the element can be included by terminating the flared slotline into a load instead of the actual feed, thus eliminating the difficulties associated with the feedline while still including coupling to the horizontally polarized element. These numerical experiments indicated that the presence of the horizontal element had little effect on the vertical (copol) element match in the simulator and so further studies did not include the horizontal elements in the model.

Numerous numerical experiments were carried out to improve element performance. These design parameters included both the stripline-to-slotline transition and the shape of the slotline flare. These simulators included hundreds of design iterations and resulted in an element design incorporating a fourth-order Marchand balun [6] for the stipline-slotline transition and a Klopfenstein–Hecken impedance taper [7] for the radiating slotline flare. The overall length of the element was approximately 23.95 mm as measured from the array aperture to the end of the slotline stub. The substrate used was 1.02-mm thick with $\epsilon_r = 2.94$. The final element design is shown in Fig. 4.

The parameters varied to optimize performance included the impedance and length of the stripline and slotline stubs in the transition region, the shape of the flare and the coupling point of the stripline-to-slotline transition. In addition, the size and shape of the posts used to hold the elements in the array were varied to determine their effect on element performance.

Once the design was finalized using computer simulations some elements were constructed for test in hardware waveguide simulators in order to validate the modeled results. The hardware waveguide simulators included only the vertical elements for the same reasons given above for the computational model. Fig. 5 shows calculated and measured results for the return loss of the final element design. Also included is the return loss for the baseline element from the previous phase of this work and the starting point for the current design. These results consist of return loss measured in three different waveguide simulators. The curves in the lower part of Fig. 5 and the right hand y axis show the H-plane scan-angle dependence with frequency in the three different simulators. Agreement between measured and calculated results is considered acceptable, especially when the coarseness of the computational model used in return for simulation speed is taken into consideration.

The RCS pattern is governed by the aperture grid, array-edge blending, element-impedance match and match variance across the aperture, element location, and other tolerances. The aperture grid was set for Bragg lobe control. Tapered conductivity "edge card" was used about the perimeter of the array to taper the aperture impedance to a conductive ground plane. This reduces RCS pattern sidelobes.

Random errors in the apertures complex reflection coefficient affect RCS pattern noise level. The reflection coefficient is affected by many parameters, dependent on the element and array feed design. Knowing the allowed RCS pattern noise level and the effect of the element parameters allows us to determine tolerances required for the element.

This design procedure was used on the test array. Element location tolerances were set at ± 0.004 in.

Impedance tolerances behind the aperture are controlled with a wide band circulator. Element location tolerances are controlled with aluminum posts integral to an aluminum aperture plate holding each individual notch element.

Fig. 6. Scanning test array.

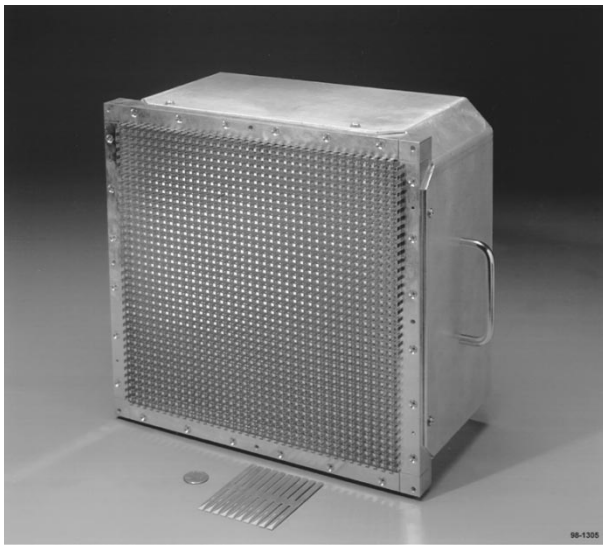

Fig. 7. RCS test array.

Two test arrays were built and tested: 1) a 10 × 10 element-active scanned beam array with eight active T/R modules and 2) a 1-ft-square passive array (terminated elements) having 37 × 37 dual-polarized elements. We measured scanned beam patterns on the former, and both element and RCS patterns on the latter. The two test arrays are illustrated in Figs. 6 and 7.

Measured performance correlated well with predicted data. Fig. 8 shows a measured scanned beam circular polarization pattern on the active test array at X band. The scan angle is 30°. Circular polarization is achieved by feeding adjacent orthogonal elements with 90° relative phase. The beam is wide because of the small array size and the sidelobe level is determined by the active element configuration. The pattern was measured with a rotating horn.

Fig. 9 shows measured H-plane element patterns at C, X, and Ku bands. Patterns show good scan coverage to 60° scan and low cross polarization. Measured RCS patterns were taken over L through Ku bands. RCS patterns show good sidelobe and noise-level performance.

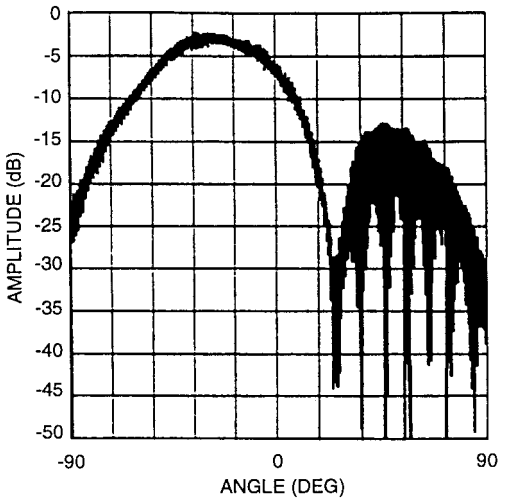

Fig. 8. Measured circularly polarized array pattern.

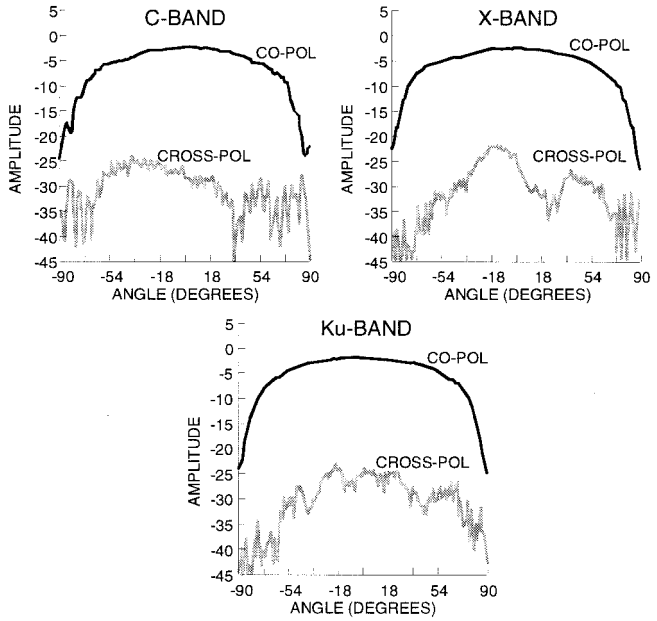

Fig. 9. Measured H-plane element pattern (in array).

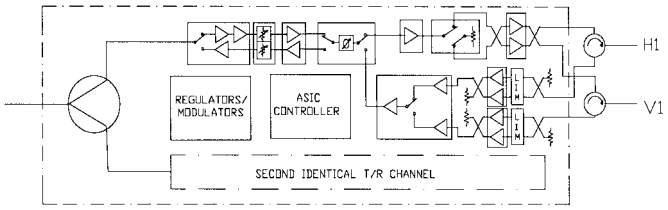

Fig. 10. T/R Module block diagram.

III. T/R Module

Fig. 10 shows a functional block diagram of the module and Fig. 11 is a photograph of the assembled 1994 prototype module with the lid removed. Size is 0.89 in wide × 0.160 high × 4.857 in long. Module width and height are set to satisfy array-element spacing for wide angle at the highest frequency. Two complete T/R functions are packaged within a single module to simplify meeting the array grid size constraints. The two T/R functions share common voltage regulator and digital controller functions, but have independent

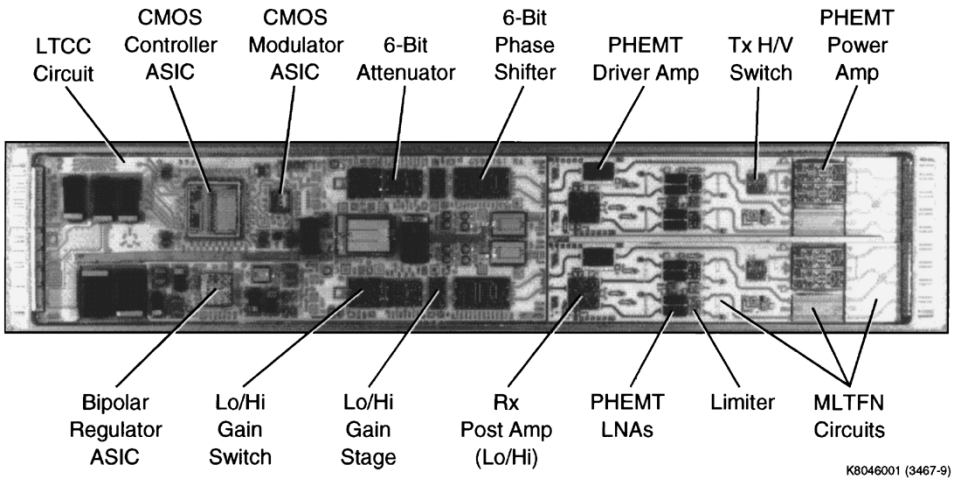

Fig. 11. T/R module photograph.

phase, amplitude, and polarization settings. At the manifold side of the module, a single RF port is used for both transmit and receive signals with a two-way combiner connecting this input to both T/R functions. Six feed through lines are for control data inputs. The module controller is configured to store up to 16 module settings (i.e., beam positions setups) to facilitate rapid switching between beams and functions.

Polarization diversity for the array is required for this wide range of applications and is achieved by having selectable linear polarization in the module. The array achieves circular polarization in selected frequency bands by operating adjacent modules in vertical and horizontal polarizations with a 90° phase offset. At the radiating element side, the module has separate transmit and receive ports for horizontal and vertical polarizations for the two T/R functions. These eight outputs connect to radiating elements through circulators. Polarization on receive is controlled by switching after the low-noise amplifier (LNA) to minimize the impact of switching losses on noise figure. The penalty for this is the complexity of two LNA front ends. Polarization on transmit is controlled by switching the driver amplifier output to alternate ports of the Lange coupler on the input side of the balanced power amplifiers. Impact of polarization switching loss on transmit efficiency is minimized.

Six-bit resolution is incorporated in the phase shifter and attenuator. The phase shifter is a "constant phase versus frequency" circuit with root mean square (rms). errors in the prototype of less than 9° in phase and less than 0.7 dB in amplitude except at the band edges. A more recent iteration of the phase shifter has rms phase error below 5°.

The average power out of the module exceeds 2.75 W over most of the band and test data shows individual modules produce 4-W output near band center. Output performance is shown across the frequency band in Fig. 12. Transmit gain is greater than 35 dB and module efficiency ranges from 5% to 10% at 45% duty factor (DF). This demonstrates an improvement over the module built in 1991 for the ASAP program which delivered 1 W over most of the band with efficiencies between 2% and 4% at 40% DF.

The receive data shown here has the benefit of a second pass-design phase shifter. As illustrated in Fig. 13, Receive

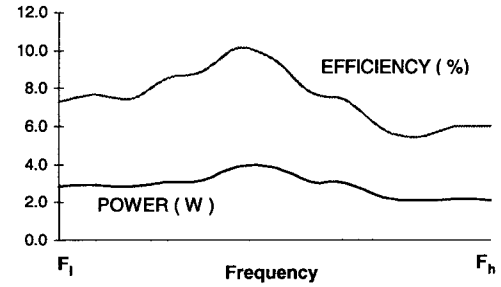

Fig. 12. Transmit performance.

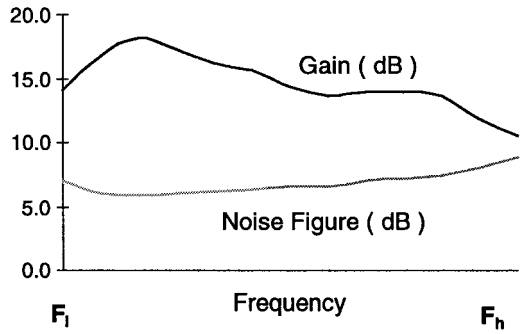

Fig. 13. Receive performance.

gain is greater than 12 dB over most of the band with a nominal noise figure of 6–7 dB.

Input third-order intercept (TOI) for the module is greater than +8 dBm across the band. Additional information on T/R module construction and circuit designs is in [8].

IV. Beamforming Network Design

A flexible beamforming network is required to support the numerous types of beams required for ASAP. Definition of the beamforming requirements for the active aperture involved selection of aperture size for each subsystem mode, e.g., use of the full elliptical aperture, a single subarray, or some intermediate aperture size. Then the transmit and receive pattern requirements were defined. In the case of radar, two-way pattern requirements are often the driving concern and there are options for allocating between transmit and receive patterns. Fifteen beam types were identified for the array in-

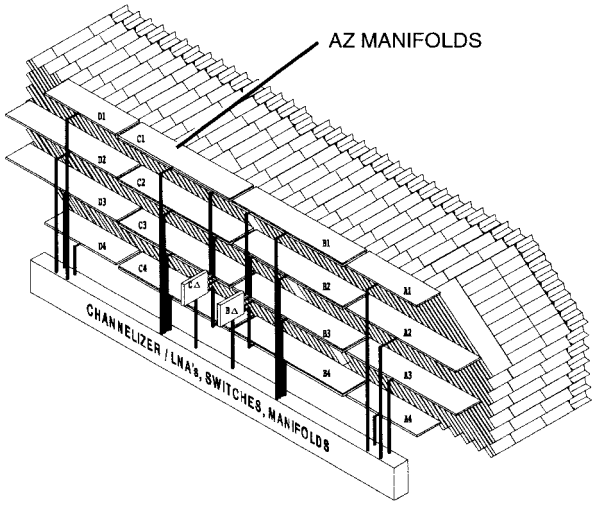

Fig. 14. Subarray manifolding.

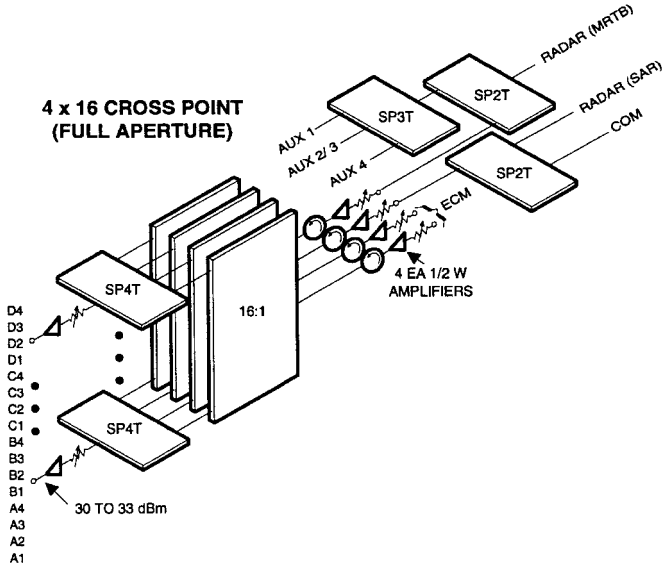

Fig. 15. Array transmit driver network.

cluding low and very low sidelobe beams and cosecant-shaped fan beams. The beam types use the full elliptical aperture or various rectangular-shaped combinations of subarrays. The array manifolding design to meet the varied beamforming requirements has a set of subarray RF manifolds implemented with uniform amplitude distributions for the subarrays, as illustrated in Fig. 14. The array packaging design is based on diagonal "slat" assemblies to allow more area for circuit layout in the T/R module. The subarray manifolding has to adapt to the diagonal design of the array slats. The subarray manifolds connect through a set of circulators to separate transmit and receive post subarray beamforming networks.

In the transmit subarray driver network, power splitters, switches, and driver amplifiers generate the signals to drive the subarrays on transmit from several different waveform sources.

A transmit driver network configuration defined for demonstration of the ASAP operation with existing radar, ECM, and communications equipment is illustrated in Fig. 15. This transmit network allows the connection of one communications, two radar, and two ECM transmit sources to the array. Up to four of these five transmit sources can operate simultaneously. The network of Fig. 15 includes a 4×16 cross-point switch network with added SP2T and SP3T switches to connect the five transmitters to the sixteen subarrays and to four wide-beam auxiliary radiating elements. This switching network meets the transmit timeline requirements of detailed tactical aircraft operating scenarios.

For receive, the signals from each subarray pass through a switchable channelizer filter unit and are then amplified in a second set of LNA's. Then the receive subarray signals are combined and switched in various combinations for output to radar (sum, azimuth difference, and elevation difference), ESM, and communications receiver functions. The receive network is somewhat more complex than the transmit and will not be detailed in this paper. For this application the network did include a capability for forming low sidelobe difference patterns for a selection for radar modes.

For both transmit and receive operations, variable attenuators in the T/R modules and in the transmit and receive post subarray beamforming networks control the aperture amplitude distribution, including setup of low sidelobe amplitude tapers. Losses in the ASAP beamforming network are higher than for more conventional phased-array radars. This does not directly degrade transmit efficiency and receive sensitivity because of the active-array configuration. The final power amplifier stages are in the T/R modules, near the radiating elements, and primarily set the transmit efficiency. The initial low noise-receive amplifier stages are also in the T/R modules, near the array elements and primarily set the receive sensitivity.

V. Time Sharing

The ASAP design described does allow simultaneous use of the aperture by more than one function at a time. However, because of coupling, simultaneous receive and transmit is not practical. On tactical aircraft with conventional antenna suites coupling is often too high for receive functions to operate, while transmitters are operating. Interconnections known as "blanking" signals are used between subsystems to control interference and mitigate the effects of coupling between antennas. These same type of controls are needed with ASAP. In the future, integrated avionics systems will be developed and it is possible that the occurance of transmit to receive interference can be minimized by an integrated system design.

Also because some radar functions require the full aperture, other transmit to receive functions must be time interleaved with these radar functions. Time-line modeling of typical tactical aircraft missions has shown that scheduling conflicts between functions occurs only occasionally and can be controlled so that performance degradation of the avionics system is small.

With a shared aperture and an integrated avionics system, resource management has been discussed in recent publications [9].

VI. Conclusions

The recently completed array and module demonstration programs described in the preceding show that the available technology supports a multi-octave bandwidth array. Associ-

ated application studies have addressed the use of broad-band shared apertures in advanced avionics system. These studies have shown that shared apertures along with advanced avionics architectures can:

- reduce the number of antennas on board the aircraft by up to 4 : 1 with a related reduction in aircraft RCS;
- reduce overall avionics size, weight, power, and cost;
- improve functional availability and performance;
- reduce the number of specialized aircraft required;
- simplify functional changes and addition of new functions.

The fabrication of a large aperture with several thousand radiating elements is the next step for the development of the ASAP concept.

ACKNOWLEDGMENT

The authors would like to thank W. Sciarretta, the project engineer for the Raytheon module design efforts. The low-temperature cofired ceramic (LTCC) substrate and several of the circuits within the T/R Module were developed by the Raytheon Co., Missile Systems Division, Tewksbury, MA.

REFERENCES

[1] R. C. Johnson, Ed., *Antenna Engineering Handbook*, 3rd ed. New York: McGraw-Hill, 1993, p. 39.24.
[2] M. Skolnik, Ed., *Radar Handbook*, 2nd ed. New York: McGraw-Hill, 1990, pp. 9.7–9.16, p. 12.17.
[3] D. Schaubert, "A class of E-plane scan blindnesses in a single-polarized arrays of tapered-slot antennas with a ground plane," *IEEE Trans. Antennas Propagat.*, vol. 44, pp. 954–959, July 1996.
[4] C. Christopoulos, *The Transmission-Line Modeling Method: TLM*. Piscataway, NJ: IEEE Press, 1995.
[5] P. W. Hannon and M. A. Balfour, "Simulation of a phased array antenna in a waveguide," *IEEE Trans. Antennas Propagat.*, vol. AP-13, pp. 342–353, May 1965.
[6] V. Trifunovic and B. Jokanovic, "Review of printed Mar.and and double Y baluns: characteristics and applications," *IEEE Trans. Microwave Theory Tech.*, vol. 42, pp. 1454–1462, Aug 1994.
[7] J. C. Coetzee and J. A. G. Malherbe, "A hybrid near-optimum impedance transition with one discontinuity," *Microwave Opt. Tech. Lett.*, vol. 3, no. 7, pp. 249–256, July 1990.
[8] A. Vespa, C. Hemmi, and W. Sciarretta, "A wideband T/R module for and airborne shared aperture array," in *Govt. Microcircuit Applicat. Conf. Dig. Papers*, Nov. 7–10, 1994, vol. XX, pp. 133–136.
[9] G. McIntire, "Shared resource management for integrated avionics," presented at AIAA/IEEE Digital Avion. Conf., Phoenix, AZ, Oct. 31–Nov. 3, 1994.

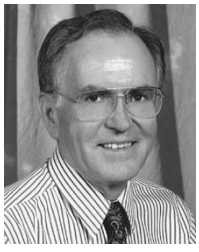

Chris Hemmi (S'62–M'66–SM'85) received the B.S. degree in electrical engineering from the University of Texas at Arlington in 1962 and the M.S. and Ph.D. degrees from the University of Texas at Austin in 1964 and 1966, respectively.

He has worked at Texas Instruments since 1966 (known as the Raytheon Systems Company since 1997) and is presently a Distinguished Member of the Technical Staff. His work has involved design development of antennas, arrays and radar and communications systems, He has worked on the architecture and design of broad-band active arrays for multifunction systems. Recently, he has been involved in design of electronically scanned arrays for satellite communications.

Dr. Hemmi is a member Eta Kappa Nu and Tau Beta Phi.

R. Thomas Dover received the B.S. degree in engineering from Case Western Reserve University, Cleveland, OH, in 1968, and the M.S. degree in electrical engineering from University of Illinois Urbana-Champaign, Urbana, IL, in 1973.

From 1968 through 1971, he worked on electrical design of manned spacecraft at McDonnell Douglas Astronautics Company, St. Louis, MO. In 1973 he joined Texas Instruments (known as the Raytheon Systems Company since 1997). He works in the Antenna/Nonmetallics Technology Center there. He has worked on both defense systems and commercial communications systems, including airborne and satellite systems His areas of interest include phased-array antenna systems and low observables..

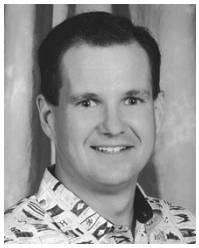

Fred German received the B.S., M.S. and Ph.D. degrees in electrical engineering, all from Auburn University, Auburn, AL, in 1986, 1987, and 1990, respectively.

From 1991 to 1992, he worked as a Summer Faculty Researcher for the Air Force School of Aerospace Medicine. He has worked at Texas Instruments Defense Systems and Electronics Group (known as Raytheon Systems Company since 1997) since 1992 in the Antenna/Nonmetallics Technology Center, where he is responsible for the analysis and design of phased-array antenna systems. His other duties involve the development and implementation of computational electromagnetic techniques and their subsequent application in the areas of antenna and microwave circuit design. He is the author of 11 technical journal publications as well as numerous conference and symposium papers.

Anthony Vespa received the B.S. degree in electrical engineering from Iowa State University, Ames, in 1964, and the M.S. degrees in electrical engineering and applied mathematics from Southern Methodist University, Dallas, TX, in 1970 and 1988, respectively.

He was employed by Collins Radio Company, Cedar Rapids, IA, from 1964 until 1972, where he designed solid-state power amplifiers in the HF, VHF, and UHF bands. He joined Texas Instruments (the Raytheon Systems Company since 1997) in 1972, where he was initially involved in RF design from UHF up through Ku-band frequencies. He was heavily involved in X- and Ku-band modules for phased-array applications. He recently has been working in the communications area as an RF Systems Engineer in the area of active personal communication system (PCS) antennas for base-station application.